

# Magnetic properties of Dy nanoparticles and Al<sub>2</sub>O<sub>3</sub>-coated Dy nanocapsules

X. G. Liu · S. W. Or · B. Li · Z. Q. Ou ·  
L. Zhang · Q. Zhang · D. Y. Geng · F. Yang ·  
D. Li · E. Brück · Z. D. Zhang

Received: 24 June 2010/Accepted: 29 September 2010/Published online: 12 October 2010  
© Springer Science+Business Media B.V. 2010

**Abstract** Dy<sub>2</sub>O<sub>3</sub>-coated Dy nanoparticles and Al<sub>2</sub>O<sub>3</sub>-coated Dy nanocapsules, with Dy cores with the average size of 3.6 and 17.6 nm, respectively, are synthesized by arc-discharge technique. The transition from ferromagnetism to antiferromagnetism absents in the Dy nanoparticles, due to that its average core size of 3.6 nm is smaller than the helix period of Dy. The temperature of the superparamagnetism–antiferromagnetism transition in the Dy nanocapsules increases abnormally to 105 K, while the Néel temperature decreases to 150 K. The magnetic

entropy change ( $-\Delta S_m$ ) of the Dy nanoparticles rapidly increases with decreasing temperature. For Al<sub>2</sub>O<sub>3</sub>-coated Dy nanocapsules,  $-\Delta S_m$  reaches 15.2 J kg<sup>-1</sup> K<sup>-1</sup> at 7.5 K, due to the existence of superparamagnetism, and a peak (5.2 J kg<sup>-1</sup> K<sup>-1</sup>) appears at 105 K due to the superparamagnetism–antiferromagnetism transition, and  $-\Delta S_m$  exceeds 2 J kg<sup>-1</sup> K<sup>-1</sup> in the temperature range from 7.5 to 105 K, for a field change from 1 to 5 T.

**Keywords** Nanoparticles · Magnetic properties · Size effect · Rare-earth metals

X. G. Liu (✉) · B. Li · Q. Zhang · D. Y. Geng ·  
F. Yang · D. Li · Z. D. Zhang  
Shenyang National Laboratory for Material Science,  
Institute of Metal Research, Chinese Academy of  
Sciences, 72 Wenhua Road, Shenyang 110016,  
People's Republic of China  
e-mail: liuxiangohugh@gmail.com

X. G. Liu · B. Li · Q. Zhang · D. Y. Geng ·  
F. Yang · D. Li · Z. D. Zhang  
International Centre for Material Physics,  
Chinese Academy of Sciences, 72 Wenhua Road,  
Shenyang 110016, People's Republic of China

X. G. Liu · S. W. Or  
Department of Electrical Engineering, The Hong Kong  
Polytechnic University, Hung Hom, Kowloon,  
Hong Kong

X. G. Liu · Z. Q. Ou · L. Zhang · E. Brück  
Fundamental Aspects of Materials and Energy Group,  
Faculty of Applied Sciences, TU Delft, Mekelweg 15,  
2629 JB Delft, The Netherlands

## Introduction

The distinctive nature of unpaired 4f electrons causes rare-earth (RE) metals possess particular physical and chemical properties, such as large magnetic moments, high electrical conductivities, and high chemical reactivity (Song et al. 2006; Kala et al. 2009). These properties enable RE elements in the form of metals, alloys, and compounds to be applied extensively in various fields, such as magnetic (Zhang 2007), magneto-optic (Schoenes 1997), magnetocaloric (Liu et al. 2008a, b), superconductive (Laurent et al. 2001), fluorescent systems (Dascalu and Dascalu 2006), nickel-RE hydride batteries (Huiberts et al. 1996), chemical temperature sensors, environment-friendly materials (Mitchell et al. 2000;

Fray et al. 2000), etc. For nanoscale RE metals, interesting optical, electronic, magnetic, and catalytic properties can be expected because of significantly increased surface area or grain boundary area (Zhang 2007). However, it is a common fact that it is extremely difficult to synthesize the nanoparticles with RE elements because of their chemical activity, which has been a nagging hindrance for their applications (Kala et al. 2009). Some efforts have been made towards synthesizing RE metals in nanocrystalline, nanoparticle, and nanopowder forms (Song et al. 2006; Wan et al. 1993; Krill et al. 1997; Shevchenko et al. 1995; Johnson et al. 1996). In most of these previous studies, RE nanoparticles were fabricated by co-sputtering RE metals in the matrix of an immiscible or low solubility material, such as, Cr, Mo, Ta, W, and Ti, followed by annealing at high temperature for precipitating RE material in nanoparticle form (Wan et al. 1993; Krill et al. 1997; Shevchenko et al. 1995; Johnson et al. 1996). Recently, Song et al. 2006 prepared bulk nanocrystalline RE (=Nd, Sm, Gd, and Tb) metals with nanograins (<20 nm) using an “oxygen-free” (oxygen concentration <0.5 ppm) in situ synthesis, where inert gas condensation was combined with spark plasma sintering in an entirely closed system. However, the complex fabrication processes and rigorous storage requirements have been the challenge for practical application of RE nanoparticles. Therefore, it is significant to search an easy and substrate-free fabrication technique, which can prevent RE nanoparticles from severe oxidization. As a well-known method for producing nanoparticles/nanocapsules, the arc-discharge technique has been widely used in the last decade (Zhang 2007; Liu et al. 2008a, b, 2009a, b; Geng et al. 2003; Zhang et al. 2006; Ma et al. 2007; Si et al. 2004). Nanocapsules, which are normally composed of a core and a shell in the size of nanometer that are made of different materials, are excellent for preventing the core from further oxidization (Zhang 2007). In the previous studies, we successfully introduced ceramics  $\text{Al}_2\text{O}_3$  as the shell and fabricated  $\text{Al}_2\text{O}_3$ -coated  $\text{REAL}_2$  ( $\text{RE} = \text{Dy}, \text{Gd}, \text{Ho}, \text{and Tb}$ ) compound nanocapsules by a modified arc discharge technique on the basis of evaporation pressures (Liu et al. 2008a, b, 2009a, b; Zhang et al. 2006; Ma et al. 2007). Recently, Gd and Dy nanocapsules,  $\text{DyCo}_2$  and  $\text{HoCo}_2$  nanoparticles were synthesized by the arc discharge technique and

their magnetic properties were investigated (Liu et al. 2009a, b, 2010; Si et al. 2004; Ma et al. 2007). These nanoparticles/nanocapsules can be stable in air without any special protection and they also exhibit large cryogenic magnetocaloric effect (MCE) induced by superparamagnetism (SPM), which can be applied for the magnetic refrigeration at low temperatures (Liu et al. 2009a, b, 2010; Ma et al. 2007, 2008). Utilization of magnetic refrigeration depends on the development of materials with sufficiently large changes of magnetic entropy at sufficiently low applied fields. In addition, from the viewpoint of application, it is highly desirable that large MCE spans over a wide temperature range. RE-based materials (including RE metals and their alloys/compounds) could exhibit the large MCE at a wide temperature range, due to their large magnetic moments, complex magnetic transitions with favorable transition temperature, which make them the focus of the research.

The dysprosium (Dy) has one of the largest magnetic moments in the lanthanide series, which reaches  $10.65 \mu_B$  (Bohr magneton) in ferromagnetically ordered state for a free trivalent ion (Herz and Kronmüller 1978). Dy exhibits numerous magnetic phase transitions as temperature and/or magnetic field vary. In a zero magnetic field, Dy is in a paramagnetic (PM) state above its Néel temperature,  $T_N = 180$  K, at which it transforms into a helical antiferromagnetic (AFM) phase stable between 90 and 180 K. Below  $T_{\text{FM-AFM}} = 90$  K, the Dy metal exhibits ferromagnetism (FM) (Chernyshov et al. 2005, 2008). The transition between the AFM and FM phases at  $T_{\text{FM-AFM}}$  is of first-order, while that between the AFM and PM states at  $T_N$  is a second-order one (Chernyshov et al. 2005). If the size of particles is comparable to fundamental magnetic lengths, confinement, and surface effects will affect the magnetic properties of the particles. Thus, nanostructured Dy is an interesting topic, especially, with respect to its variance in magnetic properties, compared with those of bulk Dy. However, due to the challenge on the synthesis, to date, few reports on the influence of reduced dimensionality on the magnetic properties of Dy nanoparticles have appeared (Herz and Kronmüller 1978; Chernyshov et al. 2005, 2008).

In this article, we synthesize  $\text{Dy}_2\text{O}_3$ -coated Dy nanoparticles and  $\text{Al}_2\text{O}_3$ -coated Dy nanocapsules by the arc discharge technique, report their magnetic

characteristics at low temperatures, and show some anomalies at different temperatures corresponding to different phase transitions. It is observed that the AFM–PM transition absents and the blocking temperature  $T_B$  presents in the Dy nanoparticles. The Dy nanoparticles display a magnetic phase transition from SPM to PM at  $T_C = 80$  K. The transition temperature  $T_{\text{SPM-AFM}}$  in the  $\text{Al}_2\text{O}_3$ -coated Dy nanocapsules increases abnormally to 105 K, while its Néel temperature  $T_N$  decreases remarkably to 150 K, compared with bulk. For the  $\text{Al}_2\text{O}_3$ -coated Dy nanocapsules, the magnetic-entropy change  $-\Delta S_m$  reaches  $15.2 \text{ J kg}^{-1} \text{ K}^{-1}$  at 7.5 K and a peak ( $5.2 \text{ J kg}^{-1} \text{ K}^{-1}$ ) appears at 105 K, for a magnetic-field change ( $\Delta B$ ) of 4 T. The former large magnetic-entropy change is contributed by the SPM, while the peak is attributed to the SPM–AFM transition.  $-\Delta S_m$  of the  $\text{Al}_2\text{O}_3$ -coated Dy nanocapsules exceeds  $2 \text{ J kg}^{-1} \text{ K}^{-1}$  for  $\Delta B = 4\text{T}$  in the temperature range from 7.5 to 105 K, which may open up a strategy of searching new materials with large MCE over a wide temperature range.

## Experimental procedure

Dy nanoparticles/nanocapsules were synthesized by a modified arc-discharge process similar to the one used in our previous study (Zhang 2007; Liu et al. 2008a, b, 2009a, b, 2010; Geng et al. 2003; Zhang et al. 2006; Ma et al. 2007, 2008; Si et al. 2004). Master DyAl alloy was prepared by arc melting Dy and Al bulks of 99.9 wt% purity under a high purity argon atmosphere. The optimum atomic properties of the button were 95 and 5 at.%, on the basis of their evaporation pressures. For the preparation of  $\text{Al}_2\text{O}_3$ -coated Dy nanocapsules, a Dy<sub>95</sub>Al<sub>5</sub> alloy ingot was used as the anode. When the base vacuum of the arc-discharging chamber reached  $6.0 \times 10^{-3}$  Pa, Ar, and H<sub>2</sub> were introduced into the chamber with partial pressures of  $2.0 \times 10^4$  and  $3.0 \times 10^3$  Pa, respectively. Then, the arc was started and the discharge current was maintained at 40 A for 2 h. After passivation with fresh Ar gas for 48 h, the product in the powder form was collected. For the preparation of Dy nanoparticles, a bulk Dy ingot was introduced as the anode under the same experimental conditions. The phase composition and the microstructure analyses of products were performed using powder X-ray

diffraction (XRD) with Cu K $\alpha$  and high-resolution transmission electron microscopy (HRTEM JEOL-2010) employing 200 kV. The oxidation behavior was investigated by thermal gravimetric analysis (TGA) and scanning differential thermal analysis (SDTA) in air atmosphere at a heating rate of  $10^\circ\text{C min}^{-1}$  from 20 to 400 °C. The magnetic measurements were carried out in a superconductor quantum interference device magnetometer (SQUID, Quantum Design MPMS-7).

## Results and discussion

The XRD patterns in Fig. 1 show the phase composition of as-prepared Dy nanoparticles/nanocapsules. As shown in Fig. 1a, except for several peaks corresponding to Dy, most of peaks in the XRD patterns can be indexed as  $\text{Dy}_2\text{O}_3$ , which reveals that the Dy nanoparticles were easily oxidized. In comparison, the XRD patterns in Fig. 1b exhibit that most of sharp reflection peaks could be indexed to Dy, in addition to several peaks indicating the existence of  $\text{Al}_2\text{O}_3$ . It is noteworthy that no other intermetallic compounds in the Dy–Al binary system and no Dy oxides are observed in the XRD patterns for  $\text{Al}_2\text{O}_3$ -

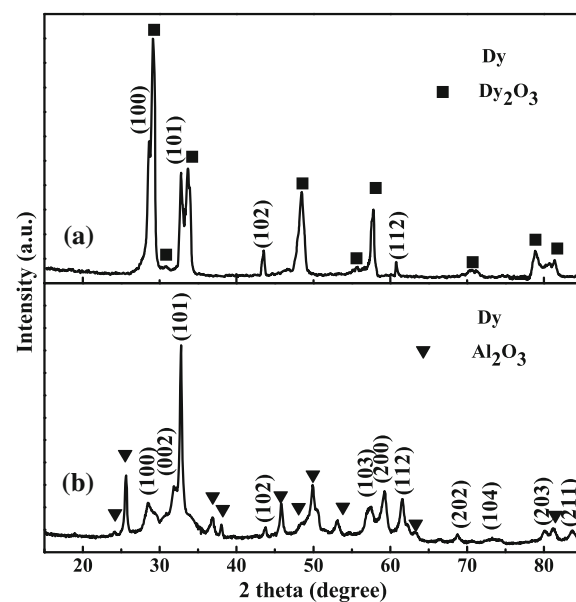


**Fig. 1** XRD patterns of **a** Dy nanoparticles and **b**  $\text{Al}_2\text{O}_3$ -coated Dy nanocapsules synthesized by the arc discharge technique

coated Dy nanocapsules. In the previous study (Zhang et al. 2006), DyAl<sub>2</sub> compound formed with different anode compositions. Thus the ratio of metal atoms in the chamber is important for the formation of the DyAl<sub>2</sub> compound in nanoscale. The absence of Dy oxides in the nanocapsules is due to the protection of Al<sub>2</sub>O<sub>3</sub>. The (101) and (102) peaks of Dy in the Dy nanoparticles are wider than those of Dy in Al<sub>2</sub>O<sub>3</sub>-coated Dy nanocapsules, which implies the smaller averaged grain size of Dy in the former. The averaged grain size of Dy in Dy nanoparticles is 3.8 nm, and that in Al<sub>2</sub>O<sub>3</sub>-coated Dy nanocapsules is 17.4 nm, according to Scherrer formula. In comparison with

those in nanoparticles, the peaks of Dy in the nanocapsules shift to higher angles, indicating the lattice shrinkage attributed to the atomic substitution. The TEM images shown in Fig. 2a and b illustrate the morphologies of nanocapsules/nanoparticles with irregular spherical shape. As shown in Fig. 3a and c, the size distribution of Dy nanocapsules/nanoparticles are 5–50 and 5–70 nm, and the average diameters are estimated as 22 and 34 nm, respectively. The size of the core in Dy nanoparticles/nanocapsules is averaged as 3.6 and 17.6 nm, respectively, according to Fig. 3d and b. It should be noted that the average size of Dy<sub>2</sub>O<sub>3</sub>-coated Dy

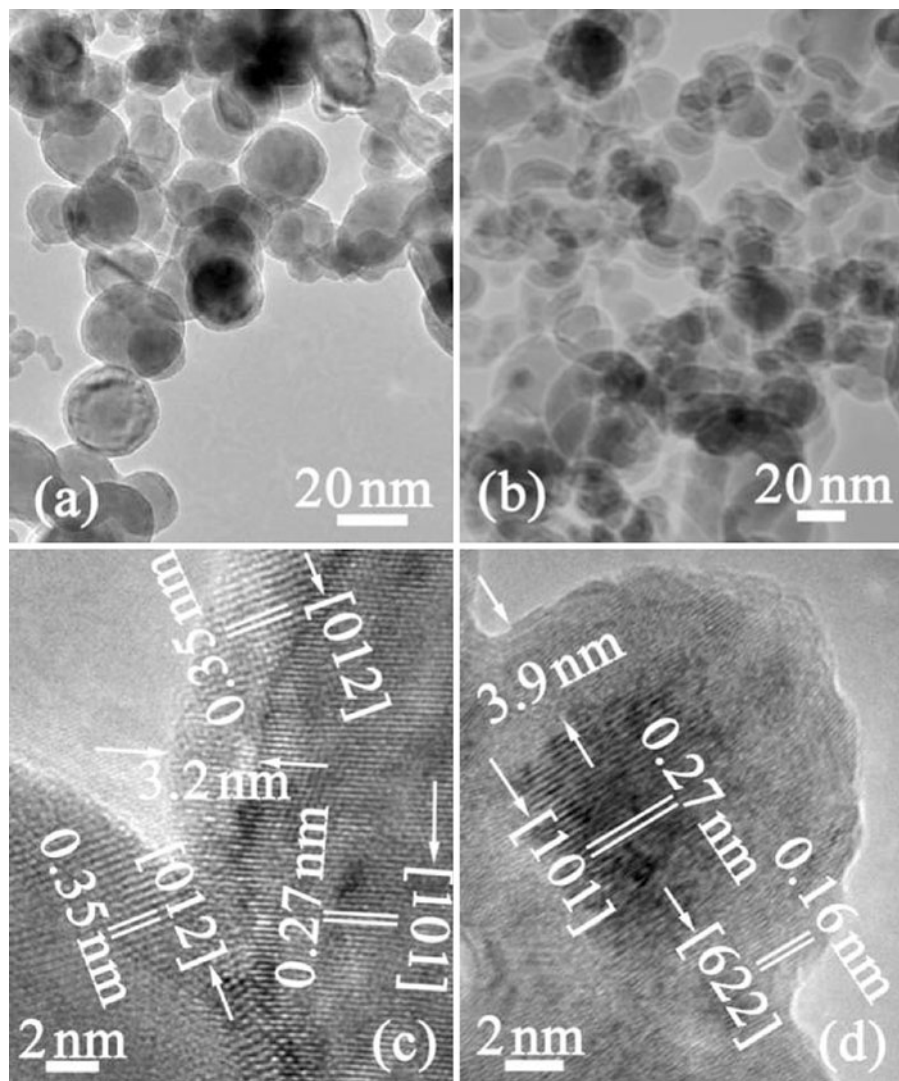


**Fig. 2** TEM images showing morphologies of **a** Dy nanocapsules and **b** Dy nanoparticles. HRTEM images of **c** a Dy nanocapsule and an Al<sub>2</sub>O<sub>3</sub> nanoparticle and **d** a Dy nanoparticle

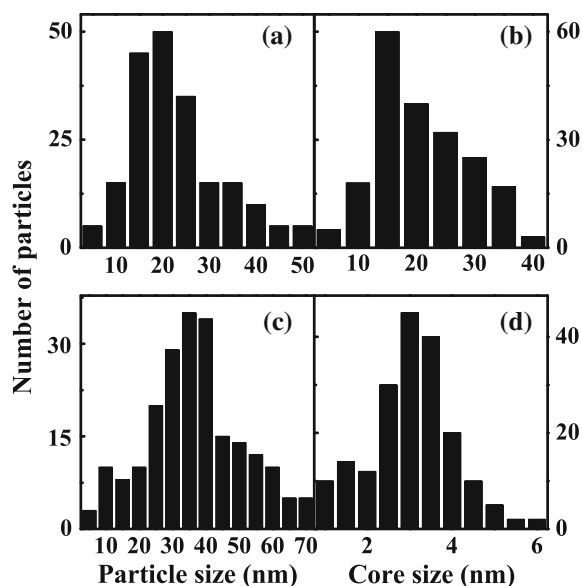


**Fig. 3** Particle size distribution of **a** Dy nanocapsules and **c** Dy nanoparticles. Core size distribution in **b** Dy nanocapsules and **d** Dy nanoparticles

nanoparticles is larger than that of  $\text{Al}_2\text{O}_3$ -coated Dy nanocapsules, while the average core size of the former is smaller than that of the latter. The size difference between the nanoparticles and nanocapsules is explained by the restrain effect of Al atoms on the growth of the nanocapsules; while the difference between the core sizes is attributed to the protection of  $\text{Al}_2\text{O}_3$  shell from further oxidation of the Dy nanoparticles in the air. The HRTEM images of a Dy nanocapsule and an  $\text{Al}_2\text{O}_3$  nanoparticle are shown in Fig. 2c. The right part of Fig. 2c shows the typical core–shell structure with a crystalline core and a shell of 3.2 nm thickness. In the crystalline core, the  $d$  spacing of 0.27 nm corresponds to the characteristic lattice distance of (101) of Dy, and the formation of the  $\text{Al}_2\text{O}_3$  shell can be confirmed by the characteristic interplane (012) spacing 0.35 nm of  $\text{Al}_2\text{O}_3$ . On the left part of Fig. 2c, however, an HRTEM image for a particle without a core–shell structure, shows the characteristic lattice fringe {012} plane with  $d$ -spacing of 0.35 nm, corresponding to  $\text{Al}_2\text{O}_3$ . It reveals that there also exists a small amount of  $\text{Al}_2\text{O}_3$  nanoparticles. The HRTEM image of a Dy nanoparticle with a typical core–shell structure is shown in Fig. 2d, in which the  $d$  spacing of 0.27 nm corresponds to the characteristic lattice distance of (101) of Dy. The 3.9-nm thick shell can be

determined as  $\text{Dy}_2\text{O}_3$  by its characteristic interplane (622) spacing of 0.16 nm.

Based on the XRD and TEM results above, the formation mechanism of the nanocapsules/nanoparticles can be briefly summarized as follows. In the arc-discharge process, the metal atoms evaporated from the anode into the chamber, in which they with a high activity reacted rapidly and then nucleated through the rapid energy exchange. The boiling point and evaporation pressure of metals determines the amount of evaporated atoms and the priority of condensed atoms. Al with its boiling point of 2740 K was more easily evaporated than Dy with a boiling point of 2835 K. When the temperature decreased, Dy atoms took the priority to be condensed. In the present experiment, Dy and Al atoms evaporated simultaneously from the  $\text{Dy}_{95}\text{Al}_5$  anode, but in a certain time, more Al atoms entered the chamber. As they had a high activity, the evaporated Dy and Al atoms rapidly exchanged energy with each other to form clusters in the high-temperature region of the plasma, which led to some Al atoms with smaller atomic radius (1.82 Å) occupy part of Dy sites with larger atomic radius 2.49 Å and cause the lattice shrinkage of Dy. When the clusters of reacted matter left the high-temperature region of the plasma, rapid quenching led to the nucleation of crystallites, and the formation of Dy nanoparticles. On the other hand, similar to the formation of  $\text{Al}_2\text{O}_3$ - and  $\text{ZnO}$ -coated Fe nanocapsules (Geng et al. 2003; Liu et al. 2009a, b), some evaporated Al atoms (fewer compared to the number of Dy atoms) were abounded on the surfaces of the Dy nanoparticles to suppress the growth of Dy nanoparticles. After passivation, Al transforms to be  $\text{Al}_2\text{O}_3$  on the surfaces of the nanocapsules to form the core–shell structure. In addition, a small number of aluminum particles formed by excessive aluminum atoms were oxidized into  $\text{Al}_2\text{O}_3$  when exposed to the air. For Dy nanoparticles, due to the large surface/ratio ratio and high chemical activity, small Dy nanoparticles and surface of big Dy nanoparticles were oxidized into  $\text{Dy}_2\text{O}_3$  when exposed to the air, which can explain why the core size in the nanoparticles is smaller than that in the nanocapsules.

It is well known that RE nanoparticles are easily oxidized or self-ignited when heated in the air. To study the thermal stability and understand anti-oxidation behavior, TGA and SDTA curves were recorded for the Dy nanoparticles/nanocapsules at a

heating rate of  $10\text{ }^{\circ}\text{C min}^{-1}$  in a flowing air atmosphere (see Fig. 4). For Dy nanoparticles/nanocapsules, the weight loss can be observed at low temperatures, due to the release of absorbed gases or moisture on the surface, and the weight exhibit a slight reduction at high temperatures above the temperature of the exothermic peak, which might be attributed to the existence of volatile matters in tube furnace (Wang et al. 2003). The weight loss ( $\sim 18.6\%$ ) in Dy nanocapsules is larger than that ( $\sim 15.2\%$ ) in Dy nanoparticles, which can be explained by the fact that the nanocapsules with smaller particle size can absorb more gases or moisture. The TGA–SDTA curves of Dy nanoparticles exhibit a gradual weight gain from 120 to  $190\text{ }^{\circ}\text{C}$ , which is associated with an exothermic peak at  $190\text{ }^{\circ}\text{C}$ , as shown in Fig. 4a. It indicates that the oxidation takes place at  $120\text{ }^{\circ}\text{C}$  and the cores have been completely oxidized to  $\text{Dy}_2\text{O}_3$  at  $190\text{ }^{\circ}\text{C}$ . It is interesting to note that in Fig. 4b, there is no weight variety from 120 to  $220\text{ }^{\circ}\text{C}$ , suggesting that Dy nanocapsules are stable in this temperature range. As

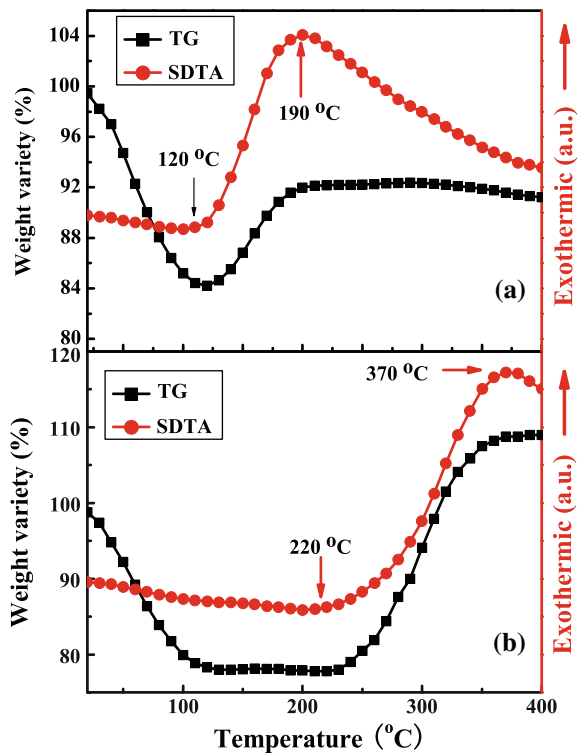
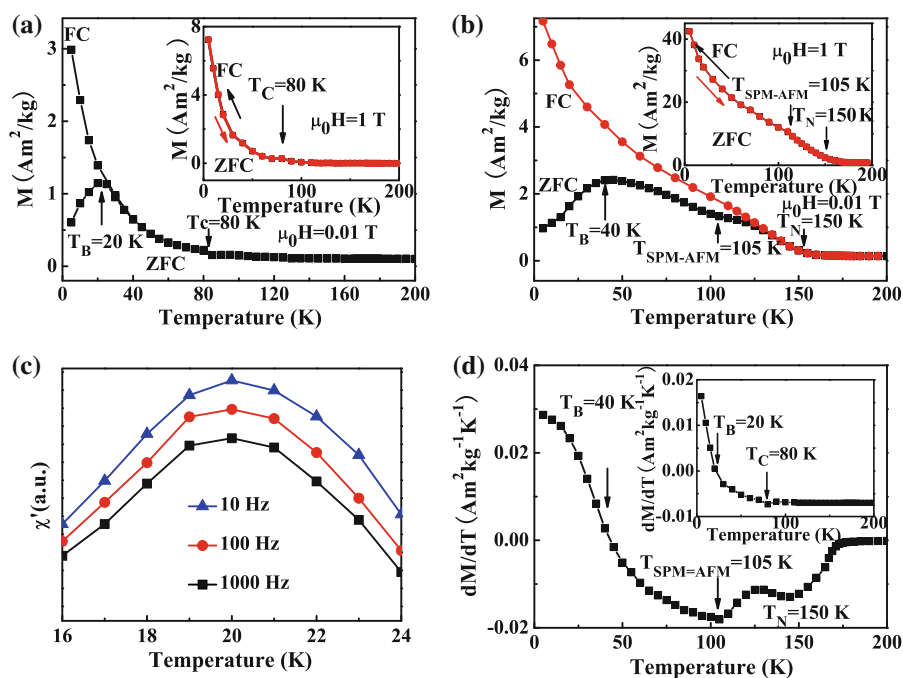


**Fig. 4** TGA and SDTA curves of **a** Dy nanoparticles and **b**  $\text{Al}_2\text{O}_3$ -coated Dy nanocapsules recorded in air with a heating rate of  $10\text{ }^{\circ}\text{C min}^{-1}$

shown in Fig. 4b, from  $220$  to  $370\text{ }^{\circ}\text{C}$ , the TGA–SDTA curves exhibit a gradual weight gain associated with an exothermic peak at  $370\text{ }^{\circ}\text{C}$ , implying that the Dy cores are slowly oxidized to  $\text{Dy}_2\text{O}_3$  from  $220\text{ }^{\circ}\text{C}$  and fully oxidized at  $370\text{ }^{\circ}\text{C}$ . It also indicates that the Dy nanocapsules are stable and secure below  $220\text{ }^{\circ}\text{C}$  in the air. The exothermic peak at  $370\text{ }^{\circ}\text{C}$  in the nanocapsules is higher than  $190\text{ }^{\circ}\text{C}$  of the nanoparticles, due to the protection of  $\text{Al}_2\text{O}_3$  shell on the Dy nanocapsules and also to the smaller core size in Dy nanoparticles.

Figure 5a and b shows the temperature dependence of the magnetization at an applied field ( $\mu_0H = 0.01\text{ T}$ ) after different cooling processes for as-prepared Dy nanoparticles/nanocapsules. In the zero-field cooling (ZFC) process, the sample was cooled from  $200$  to  $5\text{ K}$  without application of an external magnetic field, then the magnetization as a function of temperature was recorded at a relatively low applied field ( $0.01\text{ T}$ ) during the warming process. In the case of field cooling (FC), the sample was cooled from  $200$  to  $5\text{ K}$  in the presence of an external magnetic field ( $0.01\text{ T}$ ), and the magnetization as a function of temperature was recorded during the cooling process (Zhang 2007).  $\text{Dy}_2\text{O}_3$  was reported to exhibit an AFM transition with  $T_N \sim 1.2\text{ K}$ ; however, below the lowest temperature we measured (Nelson et al. 2003). Moreover,  $\text{Al}_2\text{O}_3$  exhibits PM. Consequently, the ZFC and FC curves in Fig. 5a and b show only the features of Dy nanoparticles/nanocapsules. As shown in Fig. 5a, the peak in the ZFC curve at  $20\text{ K}$  corresponds to the blocking temperature  $T_B$ , which indicates that the relaxation rate of the moments of the Dy nanoparticles decreases quickly, leading to a blocked state below  $T_B$ . The  $T_B$  of Dy nanocapsules is determined as  $40\text{ K}$  from ZFC in Fig. 5b. Higher  $T_B$  of Dy nanocapsules, in comparison with that of Dy nanoparticles, is due to the fact that larger Dy cores relax their higher moments to the same applied field at higher temperature. For Dy nanoparticles/nanocapsules, each FC curve departs from the corresponding ZFC curve at a temperature larger than  $T_B$ . Strong mutual magnetic interactions may exist in randomly distributed particles, which would induce a spin glass state in the particle system because of the spin frustration. However, the peak in the temperature dependence of the ac susceptibility in Dy nanoparticles (Fig. 5c) does not shift as the frequency is

**Fig. 5** ZFC and FC magnetization curves of **a** Dy nanoparticles and **b** Al<sub>2</sub>O<sub>3</sub>-coated Dy nanocapsules between 5 and 200 K at an applied field of 0.01 T. The insets show their corresponding ZFC and FC curves at an applied field of 1 T. **c** Temperature dependence of ac susceptibility measured at a field with a frequency 10, 100, or 1000 Hz after the ZFC process in Dy nanoparticles. **d** The first-order derivative  $dM/dT$  of the ZFC magnetization as a function of temperature in Al<sub>2</sub>O<sub>3</sub>-coated Dy nanocapsules. The inset shows the temperature dependence of  $dM/dT$  of ZFC magnetization in Dy nanoparticles



increased from 10 to 1000 Hz, which is different from the behavior of spin-glasses for which the peak would shift to lower temperatures (Liu et al. 2008a, b; Ma et al. 2007). Moreover, the value of the Curie temperature extrapolated from the reciprocal dc susceptibility obtained from FC curve of Dy nanoparticles (or nanocapsules) is 0.5 K (or 10.32 K), which is much smaller than that of systems with strong mutual interactions. These results suggest that interactions between the Dy nanoparticles/nanocapsules are very weak, because the paramagnetic shells hinder the direct contact between the magnetic cores. It is worthy noted that magnetization value at relatively low field is not well defined due to the fact that there are two different curves, i.e., FC and ZFC. However, the ZFC and FC curves overlapped with each other at an applied field of 1 T, indicating no irreversible behavior below the blocking temperature  $T_B$ , as shown in the insets of Fig. 5a and b. Moreover, the ZFC and FC curves at larger applied fields of 2, 3, 4, and 5 T also show the magnetically reversible behavior between 5 and 200 K (not shown here). As a result, the magnetic behavior of nanoparticles/nanocapsules in the ZFC and FC processes is equivalent between 1 and 5 T. Because the weak interactions will not be the most influential factor in changing the magnetization of the Dy

nanoparticles/nanocapsules between 1 and 5 T, their magnetic behavior can be described by the classical superparamagnetic theory without particles' interactions (Ma et al. 2007).

At cryogenic temperatures, bulk dysprosium is a basal plane ferromagnet with a preferred magnetic direction along the *a* axis. Its axial anisotropy is huge ( $2.5 \times 10^7 \text{ J m}^{-3}$ ) but the in-plane anisotropy  $K_6^6$  is two orders of magnitude lower,  $2.9 \times 10^5 \text{ J m}^{-3}$  (Shevchenko and Christodoulides 1999). According to the SPM theory,  $T_B$  can be described by  $25 k_B T_B = KV$ , where  $KV$  is the anisotropy energy barrier,  $k_B$  is the Boltzmann's constant;  $K$  and  $V$  are the effective anisotropy constant and the volume of the particle, respectively (Zhang 2007). For the present Dy nanoparticles/nanocapsules, the magneto-crystalline anisotropy constant  $K$  can be estimated by this formula using the blocking temperature  $T_B = 20$  and 40 K and the average core size of 3.6 and 17.6 nm, respectively, as determined experimentally above. The calculated values for  $K$  are  $6.1 \times 10^5 \text{ J m}^{-3}$  in Dy nanoparticles and  $1.5 \times 10^5 \text{ J m}^{-3}$  in Dy nanocapsules. These values are very close to the in-plane (basal) anisotropy  $K_6^6$  of bulk Dy. This causes the easy-magnetization direction to fluctuate within the basal plane and the particle to behave like a superparamagnet.

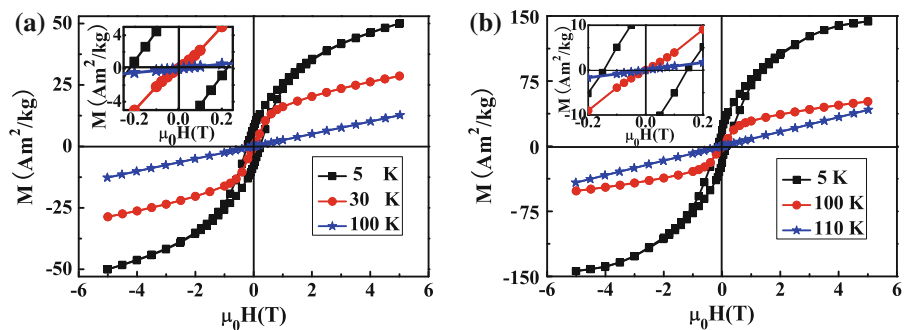
In Fig. 5a, the big turn on overlapped ZFC and FC curves at 80 K indicates the Curie temperature  $T_C$  of Dy nanoparticles, which is slightly lower than the value  $T_{FM-AFM} = 90$  K for bulk Dy. This reduction of the transition temperature is attributed to the change of intrinsic magnetic behaviors caused by the size effect and surface effect of the nanoparticles (Zhang 2007; Ma et al. 2007). The inset of Fig. 5d shows the first-order derivative  $dM/dT$  of the ZFC magnetization as a function of temperature in Dy nanoparticles. Zero value is obtained at  $T_B$ , a kink appears at  $T_C$ , and no transition can be observed at temperatures between 120 and 190 K in the inset of Fig. 5d, indicating the absence of the FM–AFM ordering transition and the AFM–PM transition appearing in bulk. This observation is in good agreement with that for Dy particles with the diameter of 4 nm and e-beam-evaporated multilayer Dy/Cu granular films of thickness 2 nm (Shevchenko and Christodoulides 1999; Tejada et al. 1994), which is ascribed to that the average core size 3.6 nm of the present Dy nanoparticles is smaller than the helix period about 4.1 nm of Dy (Mello et al. 2006).

In ZFC curve (Fig. 5b), in addition to a peak at  $T_B = 40$  K, there are two temperature ranges with abnormal decrease in the magnetization, indicative of two magnetic phase transitions. The first abnormal point in magnetization at 105 K is due to a SPM–AFM transition corresponding to the low-temperature peak of  $dM/dT$  of the ZFC magnetization (Fig. 5d); the second point at 150 K is from the AFM–PM transition corresponding to the high-temperature peak of  $dM/dT$  (Fig. 5d). Compared with bulk Dy, the Néel temperature  $T_N$  of Dy nanocapsules decreases remarkably to 150 K, while the  $T_{SPM-AFM}$  increases abnormally to 105 K. This phenomenon is similar with the shift in bulk nanocrystalline Dy with the

average grain size of 10 nm and Dy nanoparticles with the diameter of 12 nm (Shevchenko and Christodoulides 1999; Yue et al. 2008). Thinking about the average core size of 17.6 nm in Dy nanocapsules is about four times the helix period of Dy, one understands that such a deviation is due to the breaking of the helical ordering and the incomplete rotation of spins along the  $c$  axis. The stability of the helical state is modified, due to the lack of the second neighboring spins near surface region, which favors the stability of the FM order along the easy-magnetization direction with hexagonal anisotropy (Mello et al. 2006). The incomplete spin compensation, due to the lack of the second neighboring spins near the surface region in antiferromagnetically ordered materials, becomes measurable in small particle systems, where the long-range AFM order is frequently interrupted at the surfaces of the particles (Chernyshov et al. 2008). However, surface effects are not restricted to the surface. The thickness of the matter close to surface, which is modified by the surface effects, depends on the way the effective local field relaxes in the nanocapsules. In small structures, like nanoparticles/nanocapsules, the surface-to-volume ratio becomes very large with decreasing the particle size, enhancing the tangible contribution to the magnetic behavior by uncompensated spins at the surfaces (Mello et al. 2006), which causes the decrease of relaxation time of the nanocapsules gradually at the thermal agitation effects and leads to the reduction of  $T_N$ .

The hysteresis loops of the Dy nanoparticles, measured at 5, 30, and 100 K after the ZFC process, show the hysteretic characteristic (see Fig. 6a). The coercive field of 210.5 kA m<sup>-1</sup> at 5 K, which is bigger than 122.4 kA m<sup>-1</sup> for bulk Dy, indicates ferromagnetic behavior at low temperatures. But, no

**Fig. 6** **a** Hysteretic loops of Dy nanoparticles at 5, 30, and 100 K. **b** Hysteretic loops of Dy nanocapsules at 5, 100, and 110 K. The insets show the enlarged low-field part of these hysteretic loops



coercivity is observed anymore at 30 K because the Dy nanoparticles are in the SPM state. At 100 K, the magnetization increases linearly with the increase in the magnetic field, showing typical paramagnetic behavior above  $T_C$ . Therefore, the Dy nanoparticles show three kinds of magnetic behaviors between 5 and 200 K. Below  $T_B$ , Dy nanoparticles can relax their moments to the applied field within the observation of time, which makes nanoparticles show FM. From 20 to 80 K, the magnetization decreases gradually with increasing temperature, because the relaxation time of nanoparticles decreases gradually at the thermal agitation effects. Thus the particles show SPM between 20 and 80 K. Above 80 K, the thermal agitation can destroy the interaction in spins, making nanoparticles in PM state (Zhang 2007).

Figure 6b represents the hysteresis loops recorded at 5, 100, and 110 K, respectively, for  $\text{Al}_2\text{O}_3$ -coated Dy nanocapsules. Although the shape of the hysteresis loop at 5 K is similar with that in Dy nanoparticles, the magnetization ( $143.9 \text{ Am}^2/\text{kg}$ ) at 5 T is almost three times the corresponding value ( $50.1 \text{ Am}^2/\text{kg}$ ) of Dy nanoparticles and the coercive force ( $146.4 \text{ kA m}^{-1}$ ) is smaller than that ( $210.5 \text{ kA m}^{-1}$ ) in nanoparticles. This is consistent with the conclusion that the magnetization reduces and the coercive force increases with the reduction of size (Zhang 2007). Although the coercive forces of Dy nanoparticles/nanocapsules, as expected for nanosized particles, are larger than  $122.4 \text{ kA m}^{-1}$  of bulk, the relatively low coercivities are ascribed to low in-plane anisotropy, as reflected in the low blocking temperature. No coercivity can be observed in the hysteresis loop recorded at 100 K, indicating that Dy nanocapsules show SPM. From the line-like curve

recorded at 110 K and ZFC curve (Fig. 5b) and  $dM/dT$  curve (Fig. 5d), it is concluded that Dy nanocapsules are in AFM state between 105 and 150 K.

Avoiding the difference between ZFC and FC curves which is typical for nanoparticles/nanocapsules with blocking state in low applied field, the  $\Delta S_M$  of the nanoparticles/nanocapsules can be defined between 1 and 5 T. The magnetic entropy  $-\Delta S_m$  can be derived using numerical approximation  $\Delta S_m [(T_{n+1} + T_n)/2, B] = \sum [(M_{n+1} - M_n)/(T_{n+1} - T_n)] \Delta B$ , according to the Maxwell relation (Liu et al. 2008a, b; Ma et al. 2007, 2008). The  $-\Delta S_m$  of the Dy nanoparticles between 7.5 and 197.5 K upon magnetic-field changes from 1 to 5 T was calculated from the magnetic isotherms presented in the inset of Fig. 7a, in which the increment of the temperature is 10 K. As shown in Fig. 7a, the value of  $-\Delta S_m$  increases monotonously with decreasing temperature, which is similar with the results of SPM GdAl<sub>2</sub>, TbAl<sub>2</sub>, HoAl<sub>2</sub>, Gd, DyCo<sub>2</sub>, HoCo<sub>2</sub> nanocapsules/nanoparticles, due to a large magnetization change in low temperatures at a given field change (Liu et al. 2008a, b, 2009a, b, 2010; Ma et al. 2007, 2008). At 7.5 K,  $-\Delta S_m$  reaches a value of  $5.16 \text{ J kg}^{-1} \text{ K}^{-1}$  in a field change from 1 to 5 T, which is smaller than those of the systems mentioned above, due to the smaller magnetization reduced by serious oxidation in Dy nanoparticles. As shown in Fig. 7b,  $-\Delta S_m$  of  $\text{Al}_2\text{O}_3$ -coated Dy nanocapsules was calculated, according to the above formula using the magnetic isotherms in the inset of Fig. 7b.  $-\Delta S_m$  reaches  $15.2 \text{ J kg}^{-1} \text{ K}^{-1}$  at 7.5 K and a peak with the value of  $5.2 \text{ J kg}^{-1} \text{ K}^{-1}$  appears at 105 K at  $\Delta B = 4\text{T}$ . The former large value is due to the SPM and the latter peak is from the SPM–AFM transition. The  $-\Delta S_m$

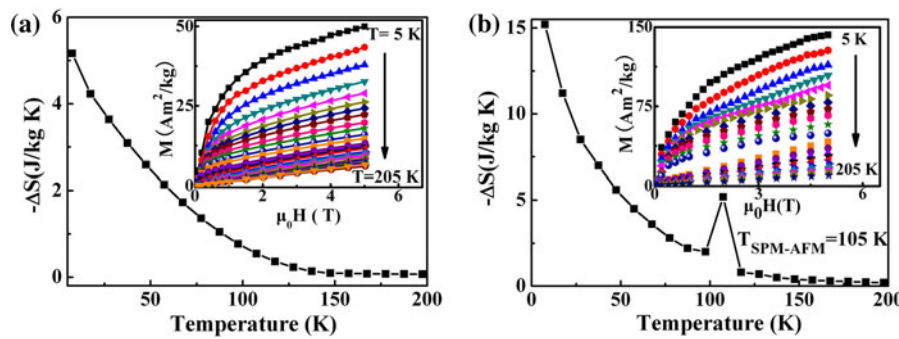


**Fig. 7** Temperature dependence of the magnetic-entropy change of **a** Dy nanoparticles and **b**  $\text{Al}_2\text{O}_3$ -coated Dy nanocapsules between 7.5 and 197.5 K in a field change from 1 to 5 T. The insets show the magnetic isotherms from 5 to 205 K, obtained in a ZFC measurement

1 to 5 T. The insets show the magnetic isotherms from 5 to 205 K, obtained in a ZFC measurement

value of Dy nanocapsules exceeds  $2 \text{ J kg}^{-1}\text{K}^{-1}$  in the range from 7.5 to 105 K at  $\Delta B = 4\text{T}$ , which is broader than that reported previously in superparamagnetic nanoparticles/nanocapsules (Liu et al. 2008a, b, 2009a, b, 2010; Ma et al. 2007, 2008; Zhang et al. 2006; Nelson et al. 2003). The wide working-temperature range mainly comes from the coexistence of the SPM and the SPM–AFM transition in Dy nanocapsules. For traditional magnetic refrigeration material, the wide working-temperature range always appears in bulk materials with two successive AF–FM and FM–PM magnetic transitions, like in Ce(Fe, Ru)<sub>2</sub>, Tb<sub>2</sub>Ni<sub>2</sub>Sn, or successively structural and magnetic transitions in Ni–Mn–In-based Hesular alloys (Chattopadhyay et al. 2006; Kumar et al. 2008; Zhang et al. 2009). It is worthwhile noting that the signs of two entropy changes in most of these materials are opposite (Chattopadhyay et al. 2006; Kumar et al. 2008), which may not fully enlarge the working temperature range since the zero MCE may be not avoided in the transition temperature range between the conventional and inverse MCE. The exception is Ho<sub>2</sub>In compound that exhibits two successive magnetic phase transitions, in which two  $-\Delta S_m$  peaks with the same sign are partly overlapping, resulting in a wide temperature interval with appreciable MCE (Zhang et al. 2009). However, MCE from SPM and SPM–AFM transition with the same sign of  $-\Delta S_m$  in the Dy nanocapsules can also enlarge the working-temperature range effectively. This study may open up a new strategy of seeking for large MCE materials over a wide temperature range. These Al<sub>2</sub>O<sub>3</sub>-coated Dy nanocapsules may serve as promising magnetocaloric material for low-temperature refrigeration applications.

The MCE is the isothermal change of entropy, which is from the variation of the magnetic moment, in a material because of an applied magnetic field (Chattopadhyay et al. 2006). The variation of the magnetization of the nanoparticles/nanocapsules is determined by the applied field Zeeman energy, thermal agitation energy  $k_B T$ , anisotropy energy barrier, and weaker interaction energy between the particles, which have different effects on the rotation of the moments, respectively. The relationship and balance among these four kinds of energies in superparamagnetic nanoparticles/nanocapsules have been studied in detail in our previous study (Liu et al. 2008a, b, 2009a, b, 2010; Ma et al. 2007, 2008;

Zhang et al. 2006). When the temperature and applied field are changed, the Zeeman energy and  $k_B T$  will help to overcome the hindrance of the anisotropy-energy barrier and the weak interaction energy to change the orientations of the large amount of magnetic moments from a high moment density in the Dy nanoparticles/nanocapsules, which can generate a large change of magnetic order and lead to a large  $-\Delta S_m$ . In addition, Dy<sub>2</sub>O<sub>3</sub> and Al<sub>2</sub>O<sub>3</sub> both are PM in measured temperature range. Although the existence of paramagnetic oxide shells (and nanoparticles) protects the Dy magnetic cores and hinders the direct contact between the magnetic cores, they also leads to the deterioration of  $-\Delta S_m$  because, when mixed with Dy nanoparticles/nanocapsules, they decrease the effective mass of the samples.

## Conclusion

Dy nanoparticles and Dy nanocapsules, in which both cores are Dy nanoparticles and shells are Dy<sub>2</sub>O<sub>3</sub> and Al<sub>2</sub>O<sub>3</sub>, respectively, have been prepared by the arc discharge. Due to the existence of Al<sub>2</sub>O<sub>3</sub> shell, Dy nanocapsules can be stable in air below 220 °C and have larger core size, compared with that of Dy nanoparticles. The magnetization (143.9 Am<sup>2</sup>/kg) of Dy nanocapsules at 5 T is almost three times the corresponding value (50.1 Am<sup>2</sup>/kg) of Dy nanoparticles and the coercive force (146.4 kA m<sup>-1</sup>) is smaller than that (210.5 kA m<sup>-1</sup>) in nanoparticles, due to the size effect. Because the average core size in the present Dy nanoparticles is smaller than the helix period of Dy, the FM–AFM ordering transition and AFM–PM transition in the corresponding bulk are not observed in Dy nanoparticles. The Dy nanoparticles exhibit three kinds of magnetic behaviors between 5 and 200 K: i.e., FM below 20 K, SPM between 20 and 80 K, PM above 80 K. Due to the breaking of the helical ordering and the incomplete rotation of spins along the *c* axis, the  $T_{\text{SPM–AFM}}$  of Dy nanocapsules abnormally increases to 105 K, while the  $T_N$  decreases dramatically to 150 K. For Dy nanoparticles,  $-\Delta S_m$  reaches a value of  $5.16 \text{ J kg}^{-1}\text{K}^{-1}$  upon a field change from 1 to 5 T at 7.5 K; For Dy nanocapsules,  $-\Delta S_m$  can reach  $15.2 \text{ J kg}^{-1}\text{K}^{-1}$  at 7.5 K at  $\Delta B = 4\text{T}$ , due to the SPM, and a peak with the value of  $5.2 \text{ J kg}^{-1}\text{K}^{-1}$  appears at 105 K, which originates from the SPM–AFM transition.  $-\Delta S_m$  of

Dy nanocapsules exceeds  $2 \text{ J kg}^{-1} \text{ K}^{-1}$  in the range from 7.5 to 105 K at  $\Delta B = 4\text{T}$ , which is broader than those reported previously in SPM nanoparticles/nanocapsules. The Dy nanocapsules may be as promising magnetocaloric material for low-temperature refrigeration applications. At the same time, this study may open up a new strategy for seeking for MCE materials over a wide working-temperature range.

**Acknowledgments** This study has been supported partly by the Science Exchange Program between China and the Netherlands, by the National Basic Research Program (No. 2010CB934603) of China, Ministry of Science and Technology of China, by the National Natural Science Foundation of China under Grant No. 50701045, and by the Hong Kong Polytechnic University Postdoctoral Fellowships Scheme (G-YX3 V).

## References

- Chattopadhyay MK, Manekar MA, Roy SB (2006) Magnetocaloric effect in  $\text{CeFe}_2$  and Ru-doped  $\text{CeFe}_2$  alloys. *J Phys D Appl Phys* 39(6):1006–1011
- Chernyshov AS, Tsokol AO, Tishin AM, Gschneidner KA Jr, Pecharsky VK (2005) Magnetic and magnetocaloric properties and the magnetic phase diagram of single-crystal dysprosium. *Phys Rev B* 71(18):184410
- Chernyshov AS, Mudryk YA, Pecharsky VK, Gschneidner KA Jr (2008) Temperature and magnetic field-dependent x-ray powder diffraction study of dysprosium. *Phys Rev B* 77(9):094132
- Dascalu T, Dascalu C (2006) Corneal collagen fibrile contraction under  $2.1 \mu\text{m}$  holmium laser irradiation. *J Optoelectron Adv Mater* 8(4):1552–1556
- Fray DJ (2000) Chemical engineering: separating rare earth elements. *Science* 289(5488):2295–2296
- Geng DY, Zhang ZD, Zhang WS, Si PZ, Zhao XG, Liu W, Hu KY, Jin ZX, Song XP (2003)  $\text{Al}_2\text{O}_3$  coated alpha-Fe solid solution nanocapsules prepared by arc discharge. *Scr Mater* 48(5):593–598
- Herz R, Kronmüller H (1978) Field-induced magnetic phase transitions in dysprosium. *J Magn Magn Mater* 9(1–3):273–275
- Huiberts JN, Griessen R, Rector JH, Wijngaarden RJ, Dekker JP, de Groot DG, Koeman NJ (1996) Yttrium and lanthanum hydride films with switchable optical properties. *Nature* 380:231–234
- Johnson D, Perera P, O’Shea MJ (1996) Finite size effects in nanoscale Tb particles. *J Appl Phys* 79(8):5299–5301
- Kala S, Mehta BR, Kruis FE, Singh VN (2009) Synthesis and oxidation stability of monosized and monocrystalline Pr nanoparticles. *J Mater Res* 24(7):2276–2285
- Krill CE, Merzoug F, Krauss W, Birringer R (1997) Magnetic properties of nanocrystalline Gd and W/Gd. *Nanostruct Mater* 9(1–8):455–458
- Kumar P, Singh NK, Suresh KG, Nigam AK (2008) Magnetocaloric and magnetotransport properties of  $\text{R}_2\text{Ni}_2\text{Sn}$  compounds ( $\text{R} = \text{Ce}, \text{Nd}, \text{Sm}, \text{Gd}$ , and  $\text{Tb}$ ). *Phys Rev B* 77(18):184411
- Laurent C, Zoltán A, Gál TP, Braun FJ, DiSalvo BB, Jürgen H (2001)  $\text{Ln}_3\text{T}_2\text{N}_6$  ( $\text{Ln} = \text{La}, \text{Ce}, \text{Pr}; \text{T} = \text{Ta}, \text{Nb}$ ), a new family of ternary nitrides isotropic to a high  $T_c$  cuprate superconductor. *J Solid State Chem* 162(1):90–95
- Liu XG, Geng DY, Du J, Ma S, Li B, Shang PJ, Zhang ZD (2008a) The large cryogenic magnetocaloric effect of  $\text{ TbAl}_2$  nanocapsules. *Scr Mater* 59(3):340–343
- Liu XG, Geng DY, Shang PJ, Meng H, Yang F, Li B, Kang DJ, Zhang ZD (2008b) Fluorescence and microwave-absorption properties of multi-functional  $\text{ZnO}$ -coated  $\alpha$ -Fe solid-solution nanocapsules. *J Phys D Appl Phys* 41(17):175006
- Liu XG, Geng DY, Zhang Q, Jiang JJ, Liu W, Zhang ZD (2009a) Microstructure and magnetic properties of graphite-coated Gd nanocapsules. *Appl Phys Lett* 94(10):103104
- Liu XG, Li B, Geng DY, Shi CX, Yang F, Kang DJ, Zhang ZD (2009b) Formation and large cryogenic magnetocaloric effect of  $\text{HoAl}_2/\text{Al}_2\text{O}_3$  nanocapsules. *J Phys D Appl Phys* 42(4):045008
- Liu XG, Geng DY, Jiang JJ, Li B, Ma S, Li D, Liu W, Zhang ZD (2010) Magnetic properties and large cryogenic low-field magnetocaloric effect of  $\text{HoCo}_2$  nanoparticles without core/shell structure. *J Nano Res* 12(4):1167–1172
- Ma S, Li WF, Li D, Xiong DK, Sun NK, Geng DY, Liu W, Zhang ZD (2007) Large cryogenic magnetocaloric effect in the blocking state of  $\text{GdAl}_2/\text{Al}_2\text{O}_3$  nanocapsules. *Phys Rev B* 76(14):144404
- Ma S, Cui WB, Li D, Sun NK, Geng DY, Jiang X, Zhang ZD (2008) Large cryogenic magnetocaloric effect of  $\text{DyCo}_2$  nanoparticles without encapsulation. *Appl Phys Lett* 92(17):173113
- Mello VD, Dantas AL, Carrico AS (2006) Magnetocaloric effect of thin Dy films. *Solid State Commun* 140(9–10):447–451
- Mitchell IR, Farrell PM, Baxter GW, Collins SF, Grattan KTV, Sun T (2000) Analysis of dopant concentration effects in praseodymium-based fluorescent fiber optic temperature sensors. *Rev Sci Instrum* 71(1):100–103
- Nelson JA, Bennett LH, Wagner MJ (2003) Dysprosium nanoparticles synthesized by alkalide reduction. *J Mater Chem* 13(4):857–860
- Schoenes J (1997) Magneto-optic lanthanide materials. *J Alloys Compd* 250(1–2):627–634
- Shevchenko NB, Murthy AS, Hadjipanayis GC (1995) Microstructural and magnetic studies of granular Gd-W films. *Mater Sci Eng A* 204(1–2):39–42
- Shevchenko NB, Christodoulides JA, Hadjipanayis GC (1999) Preparation and characterization of Dy nanoparticles. *Appl Phys Lett* 74(10):1478–1480
- Si PZ, Brück E, Zhang ZD, Škorvánek I, Kováč J, Zhang M (2004) Preparation and properties of dysprosium nanocapsules coated with boron, carbon, and dysprosium oxide. *Mater Res Bull* 39(7–8):1005–1012
- Song XY, Zhang JX, Yue M, Li ED, Zeng H, Lu ND, Zhou ML, Zuo TY (2006) Technique for preparing ultrafine nanocrystalline bulk material of pure rare-earth metals. *Adv Mater* 18(9):1210–1215

- Tejada J, Zhang XX, Ferrater C (1994) Magnetic-relaxation in very thin-films of Dy deposited onto crystalline Cu(111). *Z Phys B* 94(3):245–248
- Wan H, Tsoukatos A, Zhang YJ, Hadjipanayis GC, Shah SI (1993) Giant magnetoresist studies in (Co, Fe)-Ag films. *Nanostruct Mater* 1(1–6):399–405
- Wang ZH, Choi CJ, Kim BK, Kim JC, Zhang ZD (2003) Characterization and magnetic properties of carbon-coated cobalt nanocapsules synthesized by the chemical vapor-condensation process. *Carbon* 41(9):1751–1758
- Yue M, Wang KJ, Liu WQ, Zhang DT, Zhang JX (2008) Structure and magnetic properties of bulk nanocrystalline Dy metal prepared by spark plasma sintering. *Appl Phys Lett* 93(20):202501
- Zhang ZD (2007) Magnetic nanocapsules. *J Mater Sci Technol* 23(1):1–25
- Zhang WS, Brück E, Zhang ZD, Tegus O, Li WF, Si PZ, Geng DY, Klaasse JCP, Buschow KHJ (2006) Synthesis, structure and magnetic properties of DyAl<sub>2</sub> nanoparticles. *J Alloys Compd* 413(1–2):29–34
- Zhang Q, Cho JH, Li B, Hu WJ, Zhang ZD (2009) Magnetocaloric effect in Ho<sub>2</sub>In over a wide temperature range. *Appl Phys Lett* 94(18):182501